GEOPHYSICS, VOL. 71, NO. 6 (NOVEMBER-DECEMBER 2006); P. O77–O88, 16 FIGS., 1 TABLE.
10.1190/1.2348770

Reservoir-parameter identification using minimum relative entropy-based Bayesian inversion of seismic AVA and marine CSEM data

Zhangshuan Hou[1], Yoram Rubin[1], G. Michael Hoversten[2], Don Vasco[2], and Jinsong Chen[3]

ABSTRACT

A stochastic joint-inversion approach for estimating reservoir-fluid saturations and porosity is proposed. The approach couples seismic amplitude variation with angle (AVA) and marine controlled-source electromagnetic (CSEM) forward models into a Bayesian framework, which allows for integration of complementary information. To obtain minimally subjective prior probabilities required for the Bayesian approach, the principle of minimum relative entropy (MRE) is employed. Instead of single-value estimates provided by deterministic methods, the approach gives a probability distribution for any unknown parameter of interest, such as reservoir-fluid saturations or porosity at various locations. The distribution means, modes, and confidence intervals can be calculated, providing a more complete understanding of the uncertainty in the parameter estimates. The approach is demonstrated using synthetic and field data sets. Results show that joint inversion using seismic and EM data gives better estimates of reservoir parameters than estimates from either geophysical data set used in isolation. Moreover, a more informative prior leads to much narrower predictive intervals of the target parameters, with mean values of the posterior distributions closer to logged values.

INTRODUCTION

Estimating reservoir-fluid saturation and porosity is the goal of many geophysical surveys in hydrocarbon exploration and production. Changes in pore pressure and water saturation can be predicted when only oil and water are present (Landro, 2001). However, the presence of gas may complicate the estimation problem and may make it ill posed. This difficulty is primarily from the insensitivity of acoustic-(V_p) and shear-(V_s) wave velocities to gas saturation. According to Gassmann's equations, a gas sand with 1% gas saturation can have the same V_p/V_s as a commercial accumulation of gas (Castagna, 1993). Previous studies on the inversion of seismic amplitude variation with angle (AVA) or amplitude variation with offset (AVO) data to predict seismic parameters (Debski and Tarantola, 1995; Plessix and Bork, 2000; Buland and More, 2003) conclude that current seismic technology cannot reliably be used to distinguish economic from noneconomic gas accumulations, resulting in significant exploration losses. Regardless of this inability, seismic technology can provide two critical pieces of information needed for the ultimate estimation of gas saturation: the physical location of the reservoir unit, to within a few percent of the true values, and the porosity of the reservoir unit.

In contrast to the insensitivity of seismic attributes to gas saturation, electrical resistivity of reservoir rocks is very sensitive to gas saturation through the link to water saturation, as can be seen from Archie's law (Archie, 1942), which predicts the bulk resistivity as a function of gas saturation ($1-S_w$), as shown in Figure 1. The dependence of the bulk resistivity on gas saturation is useful for discriminating economic from noneconomic gas saturation in that the most rapid change in resistivity occurs at saturations larger than 0.7, which is mostly above the lower threshold saturation value needed for economic production.

Estimates for bulk resistivity of reservoir rocks can be obtained using marine controlled-source electromagnetic (CSEM) sounding systems, which typically consist of a ship-towed electric-dipole source and a series of seafloor-deployed recording instruments capable of recording orthogonal electric fields. Although both CSEM and passive-source magnetotelluric (MT) systems can be considered for petroleum-related exploration (Hoversten and Unsworth, 1994), CSEM systems have superior resolving capabilities when compared to MT. In the last few years, attention has been focused on the use of CSEM systems in direct detection/mapping of hydrocarbons

Manuscript received by the Editor November 22, 2005; revised manuscript received April 28, 2006; published online October 11, 2006.
[1]University of California — Berkeley, Civil and Environmental Engineering, 627 Davis Hall, Berkeley, California 94706. E-mail: hou@berkeley.edu; rubin@ce.berkeley.edu.
[2]Lawrence Berkeley National Laboratory, Earth Science Division, 1 Cyclotron Road, Mail-stop 90-1116, Berkeley, California 94720. E-mail: gmhoversten@lbl.gov; dwvasco@lbl.gov.
[3]University of California — Berkeley and Lawrence National Laboratory, Berkeley, California 94720. E-mail: jchen@lbl.gov.

(Ellingsrud et al., 2002), and a number of contractors have begun offering marine CSEM data on a commercial basis.

Because seismic and EM data have different spatial coverage and provide different images of the geology, the inclusion of EM data has the potential to improve reservoir parameter estimates over industry-standard seismic AVA techniques by providing complementary information to seismic AVA data. This is not a new idea, and studies along this line are reported (e.g., Tseng and Lee, 2001; and Hoversten et al., 2003). However, several challenges need to be addressed before such integration becomes suitable for common applications.

The major challenge is to show if and how the two different yet complementary types of data can be used beneficially. In fact, it is still a challenging issue to integrate various types of data and correctly weight their associated errors. For example, different types of data are characterized by different error levels, which are not always known prior to the inversion. Therefore, methods are needed for modeling such errors with minimum subjectivity.

Another challenge is that deterministic inversion is often an ill-posed mathematical problem because of nonuniqueness and instability. This suggests that inversion formulated in a stochastic framework (Rubin, 2003) may be more robust than traditional deterministic approaches, but additional research is needed to identify suitable stochastic formulations and to address specific issues such as computing efficiency.

Finally, incorporating prior information is not trivial. Prior information is available, in many cases, to constrain the inversion. Such information may come from geologically similar formations in the form of imprecise information such as statistical moments (means, variances, etc.) of the target parameters. Questions then arise as to what would be a rational approach for formulating such prior information within the stochastic framework.

To address these issues, we propose an entropy-based Bayesian stochastic inversion approach for estimating reservoir-fluid saturations and porosity. The approach couples seismic AVA and marine CSEM forward models into a Bayesian framework, which allows for integration between complementary information. A deterministic joint-inversion algorithm using nonlinear optimization for the same joint-inverse problem is covered in a companion paper by Hoversten et al. (2006). In this paper, we briefly compare the deterministic approach and our proposed stochastic approach.

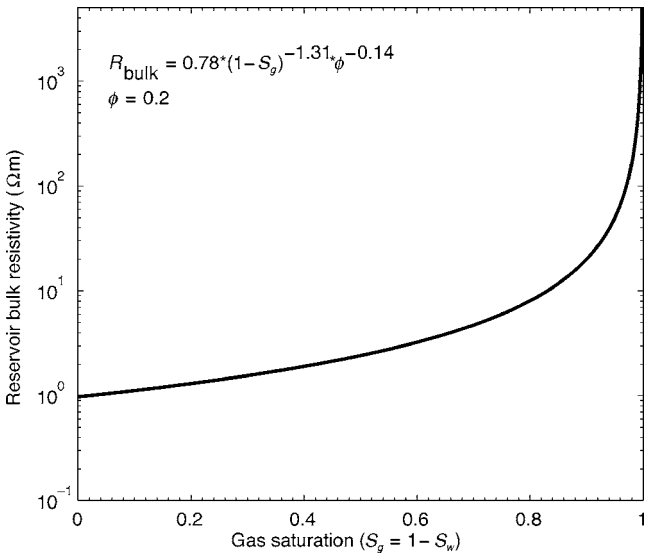

Figure 1. Reservoir bulk resistivity as a function of gas saturation (S_g) using the parameters determined from log data at the Troll field site. Porosity = 20%.

METHODOLOGY

Seismic data used for this study are prestacked angle gathers that have been normal moveout (NMO) corrected and processed to remove multiples. Marine CSEM data were collected at 24 receivers along a line across a portion of the Troll field. For our demonstration, we have used the amplitude and phase of the recorded electric field as a function of frequency and transmitter-receiver offset at one of these receivers located nearest a well that is used for comparison. The AVA data are from a common midpoint (CMP) located within 50 m of the CSEM receiver. In the joint inversion, different modeling domains for the seismic AVA and the CSEM calculations are required as illustrated in Figure 2, because of the substantial differences in the nature of energy propagation in the earth caused by a seismic source as opposed to a CSEM source. Particularly, EM energy is characterized by higher attenuation than seismic energy. After appropriate seismic processing (including amplitude recovery), one can assume that the seismic attenuation in the earth above the target interval (the overburden) has been accounted for and thus can be neglected in the seismic modeling. However, this assumption is inappropriate when modeling EM data because the effects of the overburden on the target-zone responses are large and cannot be estimated independently. Thus, EM calculations require a model with electrical conductivity described from the sea surface down (an infinite air layer is also included), while the seismic calculations only require reflection coefficients to be calculated over the area of interest.

Although attenuation in the overburden can be neglected in the seismic modeling, overburden velocities (V_p and V_s) and bulk density (ρ) above the target need to be included as parameters in seismic inversion. The reason is that a time window of the seismic AVA data is chosen in the inversion, and it is possible that the window does not exactly match the target (reservoir) zone, especially when the available velocity model used for time-to-depth conversions is not exact.

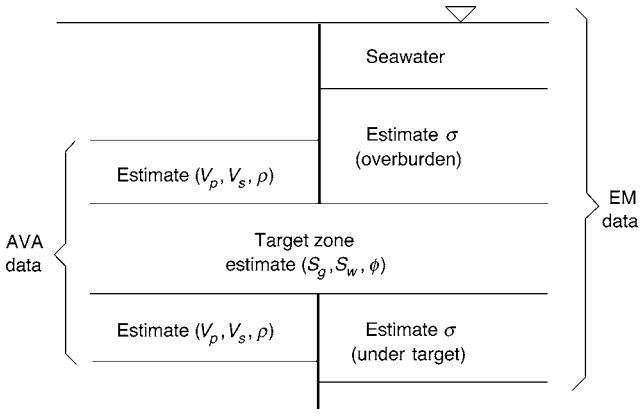

Figure 2. Schematic map of the inversion domain. The target zone is parameterized by S_g, S_w, and ϕ and is surrounded by V_p, V_s, and density zone for the AVA data and surrounded by conductivity zone for the CSEM data. The conductivity model includes the air layer for CSEM calculations.

For EM inversion, since electrical conductivities in the seawater ($\boldsymbol{\sigma}_{sea}$) and in the overburden ($\boldsymbol{\sigma}_{over}$) often have important effects on the estimation of gas saturation in the reservoir, we also consider them as unknowns. Thus, the unknowns to be inferred from seismic-data inversion include water saturation $\mathbf{S}_w$, gas saturation $\mathbf{S}_g$, oil saturation $\mathbf{S}_o$, and porosity $\boldsymbol{\phi}$ in the target zone, as well as $\mathbf{V}_p$, $\mathbf{V}_s$, and density $\boldsymbol{\rho}$ in the layers below and above the target zone. Note that $\mathbf{S}_o$ is not an independent random-variable vector, since $\mathbf{S}_o = 1 - \mathbf{S}_w - \mathbf{S}_g$. The unknowns in EM data inversion include $\mathbf{S}_w$, $\mathbf{S}_g$, $\mathbf{S}_o$, and $\boldsymbol{\phi}$ in the target zone, as well as $\boldsymbol{\sigma}_{sea}$ and $\boldsymbol{\sigma}_{over}$. The layer thickness can also be considered as unknown. Note that we use boldface letters to represent vectors.

We represent the vector of unknowns by $\mathbf{m}$. To account for parameter uncertainty, $\mathbf{m}$ is viewed as a realization of a random-variable vector $\mathbf{M}$, which is characterized by a p-variate probability-distribution function (PDF) $f_{\mathbf{M}}(\mathbf{m})$, where p is the total number of parameters in $\mathbf{M}$. The expectation of a function $g(\mathbf{m})$ (for example, the mean or variance) of $\mathbf{m}$ can be calculated as

$$\langle g(\mathbf{m})\rangle = \int_{\mathbf{m}} g(\mathbf{m}) f_{\mathbf{M}}(\mathbf{m}) d^p\mathbf{m}, \tag{1}$$

which is the integration over the entire vector space of $\mathbf{m}$.

Bayesian theory

Our approach is based on Bayes' theorem, which has previously been introduced into the field of reservoir characterization. For example, Eidsvik et al. (2002) and Buland and More (2003) develop methods for linearized seismic AVO inversion within a Bayesian framework where the posterior distributions of the target parameters are explored by Markov-chain Monte Carlo (MCMC) simulation. The Bayesian approach, coupled with the MCMC method, has been tested on both synthetic and field data sets by Chen et al. (2004), where both seismic AVA and EM data were included in the inverison without linearization.

In this study, we propose an entropy-based Bayesian approach that can quantify uncertainty as well as allow implementation of different sources of information. These sources may include prior information as well as observations such as seismic AVA and marine CSEM data. The approach determines the prior PDFs of the target parameters using the minimum relative entropy (MRE) method (Woodbury and Ulrych, 1993; Rubin, 2003; Hou and Rubin, 2005) and evaluates the posterior PDFs using a quasi-Monte Carlo method (Ueberhuber, 1997, p. 125).

For completeness, the Bayes theorem is quoted here (Rubin, 2003, chapter 13):

$$f_{\mathbf{M}|\mathbf{D},\mathbf{I}}(\mathbf{m}|\mathbf{d}^*,\mathbf{I}) = \frac{f_{\mathbf{D}|\mathbf{M},\mathbf{I}}(\mathbf{d}^*|\mathbf{m},\mathbf{I}) f_{\mathbf{M}|\mathbf{I}}(\mathbf{m}|\mathbf{I})}{\int_{\mathbf{m}} f_{\mathbf{D}|\mathbf{M},\mathbf{I}}(\mathbf{d}^*|\mathbf{m},\mathbf{I}) f_{\mathbf{M}|\mathbf{I}}(\mathbf{m}|\mathbf{I}) d^p\mathbf{m}}. \tag{2}$$

Capital letters denote random variables and lower-case letters denote their realizations. Here, $\mathbf{d}^*$ is a vector of observations, which includes both marine CSEM and seismic AVA data, and which we consider as a realization of a vector $\mathbf{D}$; $\mathbf{m}$ (a realization of $\mathbf{M}$) is a vector of order p, which includes the p parameters needed for modeling the seismic and EM responses; and $\mathbf{I}$ denotes the prior information available on $\mathbf{m}$. If we know the true values $\mathbf{m}$ of $\mathbf{M}$, we can compute the noise-free data $\mathbf{d}$ of $\mathbf{D}$ forward modeled from them. The term $f_{\mathbf{M}|\mathbf{I}}(\mathbf{m}|\mathbf{I})$ is the prior PDF of $\mathbf{m}$ given $\mathbf{I}$, $f_{\mathbf{D}|\mathbf{M},\mathbf{I}}(\mathbf{d}^*|\mathbf{m},\mathbf{I})$ is the likelihood function, and $f_{\mathbf{M}|\mathbf{D},\mathbf{I}}(\mathbf{m}|\mathbf{d}^*,\mathbf{I})$ is the posterior PDF. Simply stated, the likelihood function maps the prior into the posterior, based on the conditional PDF of the observations.

Our analysis consists of three steps. First, we model the prior by use of MRE, a systematic, analytic method that determines the prior PDF based on information such as bounds, means, or variances of the parameters with minimum subjectivity. Second, we model the likelihood function; we assume $\mathbf{d}^* = \mathbf{g}(\mathbf{m}) + \boldsymbol{\varepsilon}$, where $\mathbf{g}$ is a forward model and $\boldsymbol{\varepsilon}$ denotes the differences between observations and forward-model responses. In our analysis, $\mathbf{g}$ can be either $\mathbf{g}_1$, where $\mathbf{g}_1$ is a forward seismic AVA model, or $\mathbf{g}_2$, where $\mathbf{g}_2$ is a forward-EM model. Third, we model the posterior distributions and calculation of the corresponding statistics of the parameters using quasi-Monte Carlo integration. These steps are explained in the following sections.

Modeling the prior using MRE

The MRE method is a general approach for inferring a probability distribution from information (constraints) that incompletely characterizes that distribution. These constraints may include reasonable lower and upper bounds, i.e., averages and variances of the subsurface parameters, which can be obtained from geophysical databases or from measurements (e.g., well logs) of a few or all of the random variables in $\mathbf{M}$ at or near the study site.

The MRE solution for the prior PDF in the case where information is available in the form of the first and second statistical moments (e.g., the mean and the variance) as well as upper and lower bounds has been derived (Hou and Rubin, 2005). The prior PDF in this case assumes the form of a multivariate, truncated, Gaussian PDF:

$$f_{\mathbf{M}|\mathbf{I}}(\mathbf{m}|\mathbf{I}) = \prod_{j=1}^{p} \frac{\sqrt{\frac{\gamma_j}{\pi}} \exp\left[-\gamma_j\left(m_j + \frac{\beta_j}{2\gamma_j}\right)^2\right]}{\Phi\left[\sqrt{2\gamma_j}\left(U_j + \frac{\beta_j}{2\gamma_j}\right)\right] - \Phi\left[\sqrt{2\gamma_j}\left(L_j + \frac{\beta_j}{2\gamma_j}\right)\right]}, \tag{3}$$

where $\mathbf{I}$ represents the prior information, Φ represents the standard Gaussian cumulative-distribution function (CDF), U_j and L_j are the upper and lower bounds of parameter m_j, and β_j and γ_j are the multipliers that must be determined from the constraints, including the bounds and the moments.

The PDF represented by equation 3 has several interesting properties, making it a general solution. In the absence of bounds, $f_{\mathbf{M}_j|\mathbf{I}}(\mathbf{m}_j|\mathbf{I})$ assumes the form of the Gaussian distribution with mean $-\beta_j/(2\gamma_j)$ and variance $1/(2\gamma_j)$. If the standard deviation is large compared to the minimum difference between the expectation and the bounds, it has the form of a truncated exponential. If the variance is large and the mean is in the middle of the bounds, the PDF becomes uniform. When the variance goes to zero, then $\gamma_j \to \infty$, $\lim_{\gamma_j \to \infty} f_{\mathbf{M}_j|\mathbf{I}}(\mathbf{m}_j|\mathbf{I})$ is a delta function $\delta(\mathbf{m}_j - \mathbf{s}_j)$. When $L_j \to U_j$, the limit of the PDF is also a delta function.

The MRE PDFs may still be helpful when a bimodal distribution is possible in practice. If a distribution has two modes, when mode 1 has higher possibility than mode 2, then the prior mean is closer to mode 1 and the MRE PDF may take the form of truncated exponential, which will assign higher weight to mode 1. If the two modes have similar weights, so that the prior mean is in the middle of the bounds, the MRE PDF will be uniform, which guarantees that the values around the two modes have the similar chance to be sampled. The MRE-Bayesian approach does allow the posterior distribution to have multimodes, as shown later in the inversion results.

Moreover, when we expect bimodal distributions, covering the produced and nonproduced parts of a reservoir or in exploration the saturated and unsaturated zones, the MRE prior PDF can be generalized as $f = \mathrm{Ind}(x)f_1 + [1 - \mathrm{Ind}(x)]f2$ where Ind is an indicator variable with Ind = 1 if x is in unsaturated (or nonproduced) area. The PDF f_1 corresponds to the unsaturated (or nonproduced) area, and f_2 corresponds to saturated (or produced); f_1 is determined using the MRE method when the bounds and the prior moments are available for mode 1, so as to f_2.

Let's say we are looking at a prior in a place where $P = \mathrm{Prob}(\mathrm{Ind} = 1) = 0.4$, then the prior is $f(x|\mathrm{Ind} = 1)\mathrm{Prob}(\mathrm{Ind} = 1) + f(x|\mathrm{Ind} = 0)\mathrm{Prob}(\mathrm{Ind} = 0) = f1*0.4 + f2*0.6$. If P is unknown, we can also consider P as a random variable and derive its prior PDF using the MRE theory. Sampling from the generalized prior PDF f can be as follows:

1) generate a random sample u_0 from the distribution of P;
2) generate a random number u_1 from the [0, 1] uniform distribution;
3) if $u_0 > u_1$, we generate the sample from f_1, otherwise we use the sample from f_2;
4) repeat steps 1–3.

Forward models and the likelihood function

Forward geophysical modeling is used to estimate the likelihood function $f_{\mathbf{D}|\mathbf{M},\mathbf{I}}(\mathbf{d}^*|\mathbf{m},\mathbf{I})$. Our analysis assumes that the underlying geological structure can be represented by a layered 1D model.

For the 1D seismic AVA model $\mathbf{g}_1$, the Zoeppritz equation is used to calculate the angle-dependent reflectivity, which is convolved with an angle-dependent wavelet to form the calculated seismic AVA responses (Shuey, 1985). The modified Hashin-Shtrikman lower bounds (Hashin and Shtrikman, 1963) are used to calculate the effective moduli for porosities smaller than the critical value. This model is described by Dvorkin and Nur (1996) as applied to modeling velocity-pressure relations for North Sea sandstones, and its use in combined seismic and EM inversion is described by Hoversten et al. (2003).

For the EM forward model $\mathbf{g}_2$, we employed an integral-equation solution for the electric field from an electric-dipole source within a layered medium (Ward and Hohmann, 1987). Archie's law (Archie, 1942) is used to model electrical resistivity as a function of ϕ and S_w. The fluid bulk moduli ($K_{\mathrm{brine}}, K_{\mathrm{oil}}, K_{\mathrm{hcg}}$) and densities ($\rho_{\mathrm{brine}}, \rho_{\mathrm{oil}}, \rho_{\mathrm{hcg}}$) of brine, oil, and hydrocarbon gas, respectively, are computed using relations from Batzle and Wang (1992).

Because seismic AVA and marine EM techniques are sampling different properties over different domains, we can consider them as independent of each other. Thus, the likelihood function can be written as $f_{\mathbf{D}|\mathbf{M},\mathbf{I}}(\mathbf{d}^*|\mathbf{m},\mathbf{I}) = f_{\mathbf{D}_1|\mathbf{M},\mathbf{I}}(\mathbf{d}_1^*|\mathbf{m},\mathbf{I}) \times f_{\mathbf{D}_2|\mathbf{M},\mathbf{I}}(\mathbf{d}_2^*|\mathbf{m},\mathbf{I})$, where $\mathbf{d}_1^* = \mathbf{g}_1(\mathbf{m}) + \boldsymbol{\varepsilon}_1$ represent the observations of seismic reflectivity, and $\mathbf{d}_2^* = \mathbf{g}_2(\mathbf{m}) + \boldsymbol{\varepsilon}_2$ include amplitudes and phases of the observed electric field. The forward models can be summarized as $d_{ij}^* = g_{ij}(\mathbf{m}) + \varepsilon_{ij}$, $i = 1, \ldots, K$, $j = 1, \ldots, N_i$, where K is the number of measurement types and N_i is the number of observations for the ith type.

The likelihood function can be represented by the distributions of the errors ε_{ij}, $i = 1, \ldots, K$, $j = 1, \ldots, N_i$. Specifically, if it is assumed that ε_{ij} is characterized by a variance σ_{ij}^2 and that this is all that we know of it, the MRE principle indicates that the least prejudiced prior PDF for ε_{ij} is the Gaussian distribution. If one can assume that these distributions are independent, the likelihood function can be represented as

$$f_{\mathbf{D}|\mathbf{M},\boldsymbol{\Sigma},\mathbf{I}}(\mathbf{d}^*|\mathbf{m},\boldsymbol{\sigma},\mathbf{I}) = \prod_{i=1}^{K}\prod_{j=1}^{N_i}\left[\frac{1}{\sqrt{2\pi}\sigma_{ij}}\exp\left\{-\frac{1}{2\sigma_{ij}^2}[d_{ij}^* - g_{ij}(\mathbf{m})]^2\right\}\right]. \quad (4)$$

The posterior PDF via inverse modeling

The vector $\boldsymbol{\sigma} = (\sigma_{ij}, i = 1, \ldots, K, j = 1, \ldots, N_i)$ is generally unknown, and it is subjective to assign deterministic values to $\boldsymbol{\sigma}$ based on experiences. Here, we consider $\boldsymbol{\sigma}$ as a random-variable vector; thus, the joint PDF of $\mathbf{m}$ and $\boldsymbol{\sigma}$ can be defined using Bayes' theorem. Assuming that $\boldsymbol{\sigma}$ is independent of $\mathbf{m}$, this PDF is given by

$$f_{\mathbf{M},\boldsymbol{\Sigma}|\mathbf{D},\mathbf{I}}(\mathbf{m},\boldsymbol{\sigma}|\mathbf{d}^*,\mathbf{I}) = \frac{f_{\mathbf{D}|\mathbf{M},\boldsymbol{\Sigma},\mathbf{I}}(\mathbf{d}^*|\mathbf{m},\boldsymbol{\sigma},\mathbf{I})f_{\mathbf{M}|\mathbf{I}}(\mathbf{m}|\mathbf{I})f_{\boldsymbol{\Sigma}|\mathbf{I}}(\boldsymbol{\sigma}|\mathbf{I})}{\int_{\mathbf{m}}\int_{\boldsymbol{\sigma}} f_{\mathbf{D}|\mathbf{M},\boldsymbol{\Sigma},\mathbf{I}}(\mathbf{d}^*|\boldsymbol{m},\boldsymbol{\sigma},\mathbf{I})f_{\mathbf{M},\boldsymbol{\Sigma}|\mathbf{I}}(\mathbf{m},\boldsymbol{\sigma}|\mathbf{I})d^p\mathbf{m}d^{(N_z^*N_t)}\boldsymbol{\sigma}}. \quad (5)$$

To reduce computational demands, the dependence on $\boldsymbol{\sigma}$ can be eliminated through analytical integration of equation 5 over $\boldsymbol{\sigma}$. The significance of this step is in incorporating the uncertainty associated with $\boldsymbol{\sigma}$, while deconditioning the final results from any specific value of $\boldsymbol{\sigma}$. A conservative approach is to assume that the errors vary between zero and the upper bound of d_{ij}^*. Thus, the prior PDF $f_{\boldsymbol{\Sigma}|\mathbf{I}}(\boldsymbol{\sigma}|\mathbf{I})$ is modeled here as a uniform distribution between the bounds. Consequently, the analytical integration of equation 5 over $\boldsymbol{\sigma}$ leads to the desired posterior PDF of $\mathbf{m}$ (Hou and Rubin, 2005):

$$f_{\mathbf{M}|\mathbf{D},\mathbf{I}}(\mathbf{m}|\mathbf{d}^*,\mathbf{I}) \propto \frac{f_{\mathbf{M}|\mathbf{I}}(\mathbf{m}|\mathbf{I})\prod_{i=1}^{K}\prod_{j=1}^{N_i}\left[Ei\left\{\frac{1}{2u_{ij}^2}[d_{ij}^* - g_{ij}(\mathbf{m})]^2\right\} - Ei\left\{\frac{1}{2l_{ij}^2}[d_{ij}^* - g_{ij}(\mathbf{m})]^2\right\}\right]}{\int_m f_{\mathbf{M}|\mathbf{I}}(\mathbf{m}|\mathbf{I})\prod_{i=1}^{K}\prod_{j=1}^{N_i}\left[Ei\left\{\frac{1}{2u_{ij}^2}[d_{ij}^* - g_{ij}(\mathbf{m})]^2\right\} - Ei\left\{\frac{1}{2l_{ij}^2}[d_{ij}^* - g_{ij}(\mathbf{m})]^2\right\}\right]d^pm}, \quad (6)$$

where l_{ij} and u_{ij} are the lower and upper bounds for σ_{ij}, respectively, and Ei is the exponential-integral function, $Ei(x) = \int_x^\infty (\exp(-t)/t)dt$. Equation 6 can be used to narrow the posterior PDF and to improve our model predictions given observations $\mathbf{d}^*$.

Since the forward models of seismic AVA and marine EM data are highly nonlinear and the number of unknown parameters is large, the posterior distribution in equation 6 cannot be evaluated using con-

ventional analytical methods. Different sampling methods need to be considered instead, such as the Monte Carlo sampling method, quasi-Monte Carlo method, or importance sampling methods. The sampling strategy in this study is presented in Appendix A.

SYNTHETIC STUDIES

We illustrate our approach by using seismic and EM data inversion individually as well as jointly. A simple reservoir model assuming known rock properties is used for initial testing. The synthetic seismic and EM data sets are generated using a 1D model with 1000 m of seawater over a conductive sedimentary sequence. The target horizon is 1700 m below the seafloor. The reservoir interval comprises five 30-m-thick layers, two of which have high gas saturation. From the upper to the bottom layers, the gas saturation values are 0.1, 0.95, 0.4, 0.9, and 0.1, respectively. The corresponding porosity values are 0.15, 0.25, 0.15, 0.1, and 0.05, respectively. The synthetic AVA is sampled 50 times at 2 ms for five incident angles (0°, 10°, 20°, 30°, and 40°), calculated from the Zoeppritz equation. The synthetic EM data include the amplitude and phase of the measured electric field at 0.25 Hz for 21 source-receiver offsets. Gaussian random noise was added, starting with 10% noise (S/N ratio is 10) for the first angle and increasing up to 30% (S/N ratio is 3.3) at the far angle. Similarly, 10% Gaussian noise was added to the electric fields at the near offsets, increasing to 30% at the maximum offset. The prior bounds for the porosity and gas saturation of each layer are taken to be $[0, 0.3]$ and $[0, 1]$, respectively. This represents a uniform prior distribution of gas saturation and porosity based on entropy theory. The synthetic analysis starts with the uniform distributions to see if the inclusion of EM data can improve our estimates of reservoir parameters.

We performed a seismic-only inversion, simultaneously targeting 10 variables, including the porosity and gas saturation of the five layers. Seismic AVA inversion provides relatively accurate estimates of the porosity (see the solid curved lines in the left panels in Figure 3). In general, the uncertainty associated with the porosity estimation increases from the top to the bottom layers because the seismic data always have better coverage of the upper layers than the bottom ones. Despite the accurate estimates obtained for porosity, the seismic inversion yielded poor estimates for gas saturation, as shown in the right panels in Figure 3. This is not surprising because seismic AVA responses are less sensitive to gas saturation changes, as discussed in the introduction.

Combining both the seismic AVA and EM data in a joint inversion, we obtain the results in parameter predictions as shown in Figure 3 (dashed lines). By comparing the results with those obtained from only inverting seismic data, we can see a significant improvement for porosity at all layers. The gas saturations in layers 1 and 2 are well characterized. The predicted modes of the marginal PDFs are close to the actual values of the target variables, although the uncertainty levels in the gas saturations for layers 3∼5 are still large.

Multiple-frequency data are available (e.g., 0.25, 0.75, and 1.25 Hz) in practice. To test the inversion performance with more information included, we generated EM synthetic data at three frequencies common in field data. The inversion results are shown in Figure 3 in dotted lines, from which we can see that the joint inversion using seismic and multiple-frequency EM data provides better estimates of gas saturation at all layers. Although the uncertainty levels for the bottom layers remain significant, the modes of the PDFs are closer to the true values, thus all gas-rich or water-rich layers are identified. As stated above, up to 30% noise has been introduced into both measurements and the forward-model responses; thus, large predictive bounds are not unexpected.

In synthetic analyses, it is also interesting to explore conditions that are less favorable for joint inversion and to estimate the error level in the data that makes the joint inversion nonbeneficial. In the following study, we work on a different synthetic model by flipping the target layers upside down, such that the top layers are more resistive with high gas saturation; the contrast between adjacent layers is much less compared to the original synthetic case. Specifically, from the upper to the bottom layers, the gas saturation values are 0.95, 0.9, 0.05, 0.1, and 0.4, respectively. The corresponding reference porosity values are 0.25, 0.1, 0.15, 0.05, and 0.15, respectively. As shown in Figure 4, we obtain good estimates of the porosity at all layers and the gas saturation in the top gas-rich layers of the target zone. However, because of the existence of the resistive layers on the top of the target zone, the CSEM and the seismic AVA responses become less sensitive to changes in the gas saturation at bottom layers; meanwhile, the gas saturation has less contrast between adjacent layers. As a result, the gas saturation at the bottom layers is not well identified. This study shows that the joint-inversion results using seismic AVA and EM data could be compromised under unfavorable conditions, for example, with resistive layers on top or with weak contrast in target parameters between adjacent blocks. Under these situations, the EM and seismic AVA responses are not sensitive to changes in target parameters.

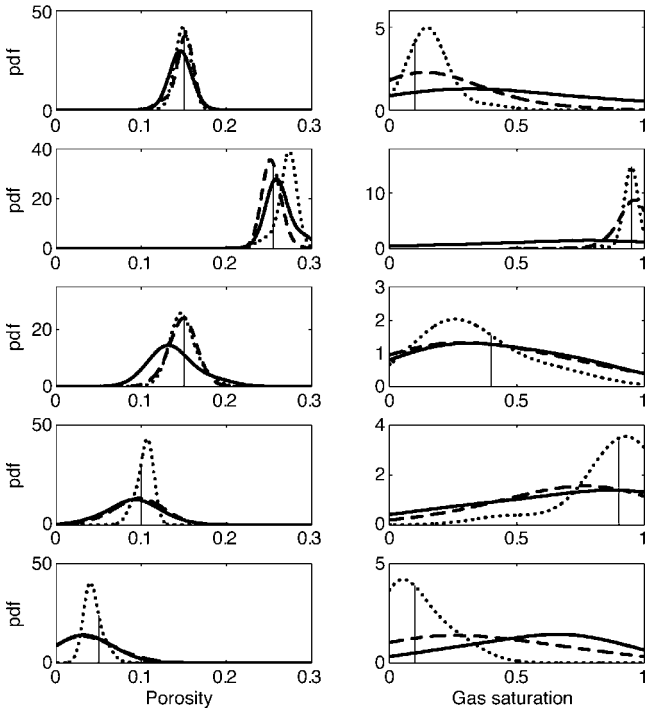

Figure 3. Estimated porosity and gas saturation. The solid curved lines represent the estimated PDFs using seismic AVA data only. The dashed lines represent estimates using both seismic AVA and 0.25-Hz CSEM data. And the dotted lines represent estimates using seismic AVA and multiple-frequency (0.25, 0.75, and 1.25 Hz) CSEM data. The vertical lines represent the true values. The plots to the left are the estimates of porosity at layers 1∼5 (from top to bottom). The plots to the right are the estimates of gas saturations at layers 1∼5 (from top to bottom).

We perform similar inversion analyses using synthetic data generated using various true models and associated with different error levels. In general, the inclusion of EM data improves our ability to identify the gas-rich layers, although the improvements may vary given different locations of gas-rich and water-rich layers. When the error levels associated with the EM data are very high (e.g., the S/N ratio is around three or even smaller at the near offset), the joint-inversion results converge to that of seismic AVA only inversion, thus making the inclusion of EM data nonbeneficial. Moreover, when the S/N ratio is around two or even smaller at small incident angle for the seismic AVA data, even the porosities cannot be identified.

TROLL FIELD STUDIES

In this section, we apply our MRE-based Bayesian approach to the Troll field site, the location of which is shown in Figure 5. The Troll field is located in the North Sea, near the west coast of Norway, on the edge of the Horda Platform. The field is divided by two major north-south-trending faults that separate the field into three provinces; Troll West Oil Province (TWOP), Troll West Gas Province (TWGP), and Troll East. Our study site is located at TWGP, where seismic and marine CSEM data are available, since 2003. The marine CSEM line from receivers 1 to 24 is shown as the straight line in the southwest direction in Figure 6. Also shown in Figure 6 is the simplified geological cross section below the CSEM transect. The reservoir interval is Jurassic sandstones, with a thick gas column. Hydrocarbon-filled sands show high average resistivities, between 200 and 500 Ωm, and occur at a depth of about 1400 m below sea level. Water-bearing sandstones, sands, and overburden sediments show resistivities in the 0.5–2-Ωm range (Johansen et al., 2005). Besides the high reservoir resistivities, the well-defined field edges, the low and relatively constant resistivities in the geological layers above the reservoir, and the moderate distribution of the hydrocarbon-filled reservoir, the TWGP site is also characterized by the smooth seafloor and the constant water depth. These characteristics make it well suited for testing our seismic and EM inversion approaches, with the assumption that the actual earth can be represented by a 1D layered model. There are several boreholes available around the TWGP site, and well 31/2-1 intersects the reservoir beneath the CSEM transect near receiver 16. The small area near receiver 16 is chosen as our study site because the well-log data can provide prior information about the reservoir parameters or provide information for model evaluation.

A well located approximately 4 km to the northeast of our survey line was used to derive all the parameters of the rock-properties model, described in Hoversten et al. (2006). This well was also used to derive the angle-dependent wavelets used in the AVA modeling of the seismic data at the CMP nearest receiver 16.

The 3D seismic data used in this study are migrated and sorted into CMP gathers. NMO and residual NMO were applied, along with multiple removal and filtering to a nominal zero-phase wavelet. The CMP-gather offsets were converted to angles by ray tracing in a layered model with velocity and density taken from well 31/2-1.

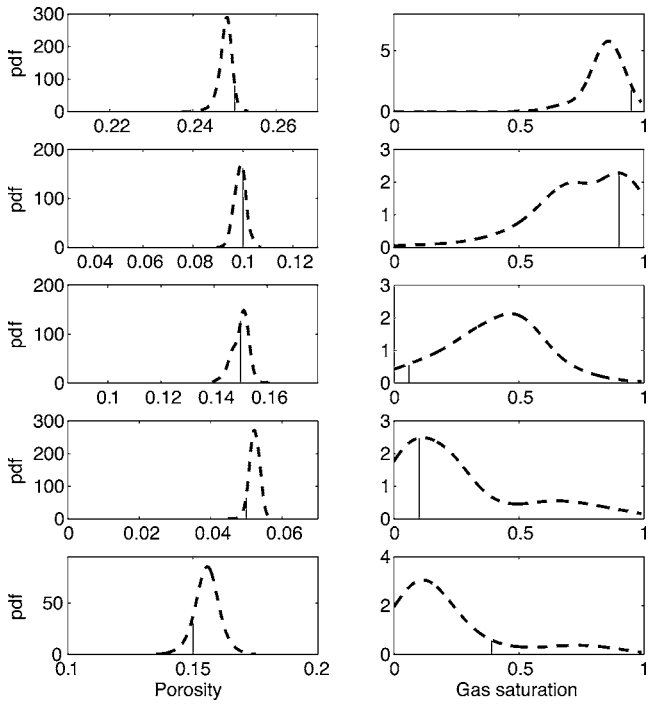

Figure 4. Estimated porosity and gas saturation using seismic AVA and multiple-frequency (0.25 Hz, 0.75 Hz, and 1.25 Hz) CSEM data. The vertical lines represent the true values. A different true model is assumed by flipping the target layers upside down.

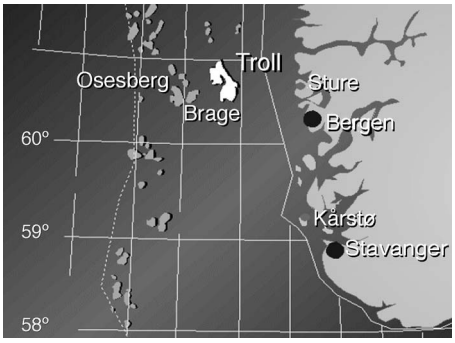

Figure 5. Location map of Troll field site (Leiknes et al.).

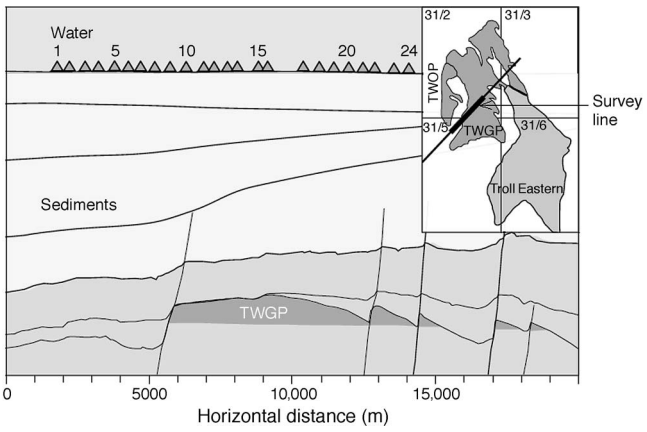

Figure 6. Simplified geological cross section along the CSEM survey line in the Troll West Gas Province (TWGP) (after Johansen et al., 2005). The marine CSEM line from receivers 1 to 24 is shown as the straight line in the southwest direction in the inset. The large panel gives the locations of the CSEM receivers along the survey line. The receivers are deployed from southwest to northeast along the line. Well 31/2-1 intersects the reservoir beneath the CSEM transect between receivers 16 and 17.

Depth-time pairs were generated from well 31/2-1 and used to determine the time window for the seismic data such that the data covered the depth interval 100 m above and below the reservoir zone (Hoversten et al., 2006).

Marine EM data used in this study consist of amplitude and phase as a function of frequency and transmitter-receiver offset at receiver 16, the closest receiver to the well. Receivers 1 to 24 are placed along the CSEM survey line from southwest to northeast, with nominal separation between receivers of 750 m along the line. A 220-m electric-dipole transmitter, producing 800 amps, was towed at approximately 2 knots along the receiver line in both directions, producing data at the receivers for transmitters on either side of the receiver. The EM amplitudes and phases along with the applied current and transmitter locations are recorded as time series, which are then averaged to produce in-phase and out-of-phase electric field for average transmitter locations spaced 100 m apart along the line. The data are recorded at three frequencies: 0.25, 0.75 , and 1.25 Hz.

Figure 7 shows the CSEM data converted to amplitude and phase of the electric field in the line direction (roughly parallel to the transmitter dipole orientation) for receiver 16. If the earth had a 1D conductivity structure (as the inversion forward model assumes), the response, both amplitude and phase, would be identical for transmitters on either side of the receiver. We see that this is true for offsets up to about 4 km. Beyond 4 km, the difference between data from transmitters on either side of the receiver increases with offset and frequency. The largest asymmetry occurs for the highest frequency at the far offsets in both amplitude and phase.

In general, the spatial sensitivity of the CSEM data to this dipole-dipole configuration is a function of source-receiver offset, earth conductivity, and frequency, with lower frequencies and larger offsets having sensitivity to deeper changes (Spies, 1989). As the transmitter-receiver offset increases, the centroid of the sensitivity region moves downward and away from the receiver in the direction toward the transmitter. To approximate a 1D response, we have averaged the EM data for transmitters on either side of the receiver, thus causing the centroid of the sensitivity region of the averaged data to be directly below the receiver location.

The water depth over the survey area is 320 m. In general, the magnitude of the response from resistive zones in the subsurface as a percentage of the total observed field becomes less as the water depth decreases. This is caused by the increased magnitude of the direct air wave, that portion of the total field that propagates up through the water, through the air, and back down to the receivers. In principle, if the seafloor bathymetry and seawater conductivity are well known, this effect can be incorporated in the modeling so that inversion of the data can accurately image the subsurface. In practice, there is some noise floor below which the target response cannot be extracted from the total field. The list of noise includes, but is not limited to, incorrect assumptions about water conductivity, incorrect positioning of sources and receivers, and errors in transmitter current magnitude and phase. The determination of when the water depth is too shallow must be done on a site-by-site basis and is dependent on the size, resistivity, and depth of the target. In the case presented here, the resistive section of the Troll field is over 100 m thick at a depth of 1400 m, and forward modeling shows that the reservoir produces a contribution to the total field that is approximately 25% at an offset of 5 km, which is 1 km before the air wave begins to dominate the response.

In addition to the seismic and EM data, V_p, S_w, density, and porosity logs are available from well 31/2-1. No production has occurred in the area near the well, so we expect that S_w has not changed by more than 1% or 2% since the logs were taken. The well log also shows a predominantly oil zone between 1544.5 and 1557.5 m depth, where original oil saturations were between 70% and 85%. Below 1557.5 m depth is a paleo-oil zone, where original oil saturations were 20% to 30%. No gas- or oil-saturation logs are available, but time-lapse seismic data have been interpreted as follows: Between the time of log measurements and the geophysical survey data used in this study, production from the oil rim has lowered reservoir pressures such that gas has been released from the oil in the oil and paleo-oil zones, resulting in a 5% increase in gas saturation in these zones (Hoversten et al., 2006). We therefore use the logged S_w to calculate oil and gas saturation in the reservoir as follows: Above 1544.5 m depth, oil saturation (S_o) is assumed to be zero thus, $S_g = 1 - S_w$. Below 1544.5 m, $S_g = 0.05$ thus, $S_o = 1 - S_w - 0.05$. The logged S_w and calculated S_g and S_o are used for comparing the performance of the different inversions.

The Bayesian model in equation 2 for this application was developed based on the geometry shown in Figure 2. We divide the reservoir into 16 layers, each of which has a thickness of 20 m. The unknowns are S_w, S_g, S_o, and ϕ for each of these target layers. For seismic AVA data inversion, we also consider V_p, V_s, and ρ as unknowns for the five layers above and the one layer below the reservoir, with each layer having a thickness of 20 m. For EM data inversion, we also include among the unknowns the electrical conductivity at each layer of the reservoir overburden (including seawater), which is divided into 13 layers based on resistivity logs collected from well 31/2-1.

Overburden V_p, V_s, and ρ above the target zone are required for two reasons. First, the time interval for the seismic data used in the inversion is chosen from a time-to-depth conversion based on the available velocity model, which may be in error. If the depth to the top of the target (reservoir) zone does not exactly tie to the selected time window, the inversion can adjust V_p above the target zone as a correction. Second, log information required to calculate the rock-properties model is usually only taken within the reservoir, so that we can only describe the target zone itself in terms of fluid satura-

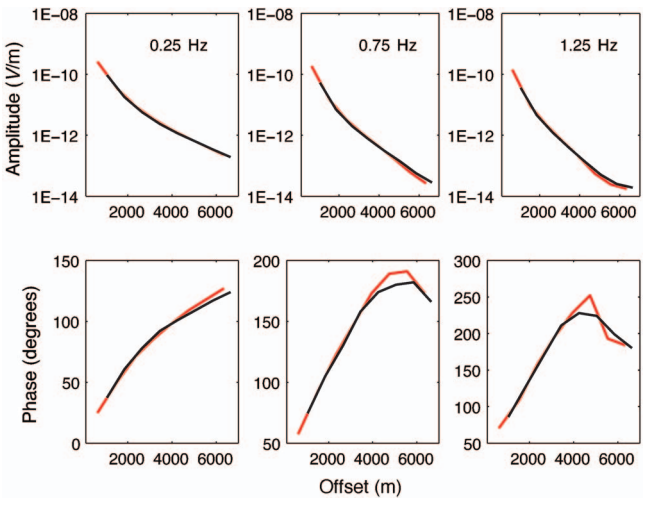

Figure 7. Electric-field amplitude (upper row) and phase (lower row) at 0.25, 0.75, and 1.25 Hz as a function of the source-receiver offset (m) at CSEM receiver near well 31/2-1. Transmitter locations to the west of the receiver are plotted in black; transmitter locations to the east are plotted in red.

tions and ϕ. However, we need properties for the layer directly above the reservoir to calculate the reflection coefficient at the top of the reservoir. The V_p, V_s, and ρ below the target interval are not strictly required but provide continuity in the seismic data fit at times below the reservoir.

We adopt relatively wide bounds for all these parameters in the following ways. For the parameters in the zones outside the reservoir, such as V_p, V_s, and ρ at the layers below and above the reservoir, as well as the electrical resistivity of the overburden layers, we assume they vary within 20% of the interval averages from well 31/2 -1. For S_w and S_g, we set their bounds at ±0.3 from linear trends, with S_g trending from one to zero, while S_w trends from zero to 0.8, going from the top to the base of the reservoir. The upper bound on S_o is set to be 0.1 above 1544.5 m depth, where no oil was present in the original logs; while below 1544.5 m, where oil was originally present, the S_o upper bound begins at 1 at 1544.5 m and decreases linearly to 0.3 at the base of the reservoir. The bounds for ϕ at the target layers are set at ±0.1 from their initial interval-averaged well-log values. All of these bounds are subject to the physical constraints on the relevant parameters; for example, the bounds for S_w, S_g, S_o, and ϕ should be within the interval $[0, 1]$.

Inversion results using uniform priors

As mentioned above, the MRE approach is used to determine the prior distributions of these unknown parameters, given the prior information such as the bounds and moments of the parameters. Assuming the bounds on the target parameters are all the information we have, the priors take the form of uniform distributions based on entropy theory, as shown in equation 3.

Using the uniform prior distributions, we performed an inversion using only the seismic data from the CMP gather at receiver 16; the results are shown in Figure 8. The red symbols are the borehole logs, the green lines are the prior bounds, the blue lines represent the estimated posterior modes, and the black dashed lines represent 0.5% and 99.5% quantiles of predictions (99% predictive intervals). From Figure 8, we can see that the predicted porosities are close to the logged values. Compared to the prior bounds, the predictive intervals show that the predicted uncertainty decreases.

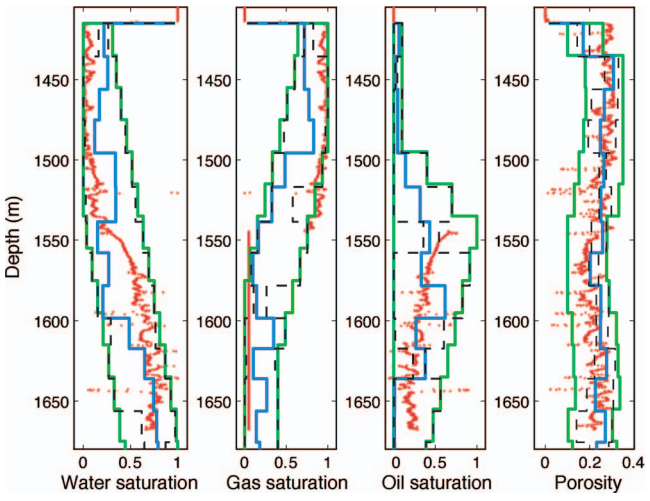

Figure 8. Inversion using seismic data only. Red dotted lines represent well-log values, green lines are the prior bounds, blue lines are the estimated posterior modes, and black lines represent 99% predictive intervals.

The water saturations at the target layers are not well identified, and the predictive intervals are almost the same as the prior bounds. Consequently, the uncertainty levels associated with both the gas saturation and the oil saturation at almost all target layers are not reduced. These results are reasonable because seismic responses are more sensitive to porosity but are less sensitive to water, gas, or oil saturations. For S_w, S_g, S_o, and ϕ, the rms of the misfits between the inverted-parameter values (posterior modes) and the well-log observations is 0.724. Our method calculates posterior distributions instead of specific values such as posterior modes. Although both the rms misfit and the predictive intervals are used to evaluate the goodness of the inversion results, we consider the latter to be more informative.

The seismic AVA model responses calculated using the posterior modes of the parameters are shown in Figure 9, together with the observed seismic data and the differences between model responses and observations. From the figure, we can see that the modeled seismic AVA responses match the observations very well. To facilitate the comparison of the results using different inversion approaches, we also calculated the rms of the differences between the modeled seismic AVA responses and the observations. The rms seismic data misfit in this case is 0.766, which was normalized by the maximum value of seismic observations.

Figure 10 shows the inversion results using only the EM data at receiver 16 (Rx16). The uncertainty levels associated with both water saturations and porosity at the target layers are not reduced. Although the posterior modes of water saturations at top layers and porosity at middle layers are close to the well logs, the corresponding predictive intervals are too large to make the predictions convincing. Moreover, the high water saturations between the depth of 1560 m and 1640 m are not identified. These results are compatible with our synthetic case studies; the estimation of porosity and water satura-

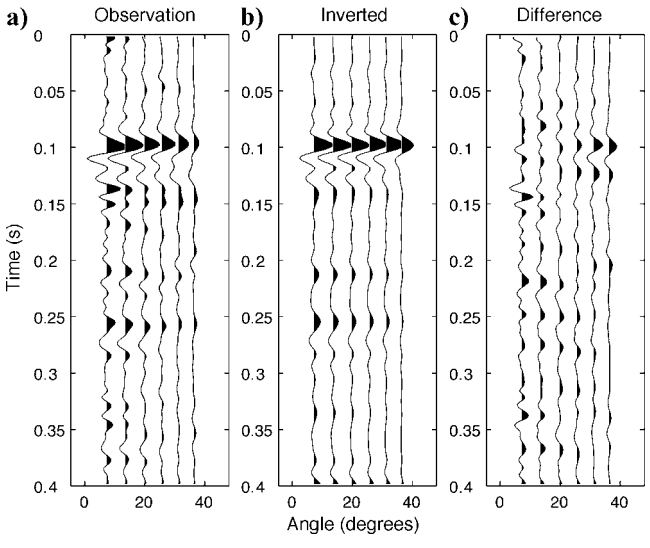

Figure 9. (a) Observed seismic AVA gather, (b) calculated AVA data from seismic-only inversion, and (c) the difference between observed and calculated AVA data. Zero time corresponds to the top of the seismic-inversion zone 100 m above the reservoir. The top and base of the reservoir are at 0.1 and 0.37 s, respectively.

tion using only EM data is poor because the EM responses are affected by porosity and water saturation simultaneously and their effects cannot be separated.

The EM observations and the calculated model responses based on the posterior modes of the parameters are plotted in Figure 11. The EM model responses calculated from the estimated parameters match the observed amplitudes well at all frequencies. However, the matches between the calculated and observed phases are not good at further offset. The reason could be that the EM data are influenced by the heterogeneity of the reservoir, the effect of which is amplified at the larger offsets; therefore, the 1D layered-model assumption becomes inappropriate compared to the smaller offsets. Moreover, the phase matches are better for lower-frequency EM data because higher-frequency EM data have higher resolution and thus are more easily influenced by the heterogeneity between the sea surface and the bottom of the reservoir. Considering that the EM observations range over several orders of magnitude, we normalized the misfits by the EM observations (relative misfits = misfits/observations), and the corresponding rms value of the relative misfits is 0.217.

Figure 12 shows the inversion results for joint inversion using the EM and seismic AVA data simultaneously. Compared to the results using seismic data only, the posterior modes of water saturations from joint inversion are much closer to the well logs for the target layers: the corresponding rms misfit of water saturation decreases from 0.212 to 0.170. The achieved rms misfits for S_w and S_o, as well as the total misfit, are smaller than those obtained using nonlinear least-squared approach by Hoversten et al. (2006). The estimates of the gas saturations for the upper half of the reservoir layers are also improved. However, the predictive intervals are still large. These results indicate that the parameter estimation at the target layers can be improved with the inclusion of EM data, but the uncertainty levels of these parameters remain high given the relative noninformative prior bounds.

Inversion results using truncated exponential priors

In application, more information on the reservoir parameters may be available, for example, their expectation values (prior means). Given information about the bounds and the prior means, the priors take the form of truncated exponential distributions based on MRE theory (Woodbury and Ulrych, 1993; Rubin, 2003; Hou and Rubin, 2005). The prior means can be obtained from other sites explored in this province. To show how this additional information can be used to improve our parameter estimation, we use the values from the linear trends as the prior means, with S_g trending from one to zero and S_w trending from zero to 0.8, considering the possible presence of oil near the base of the reservoir.

Using the truncated exponential priors, we performed inversions using seismic AVA data and EM data individually, as well as a joint

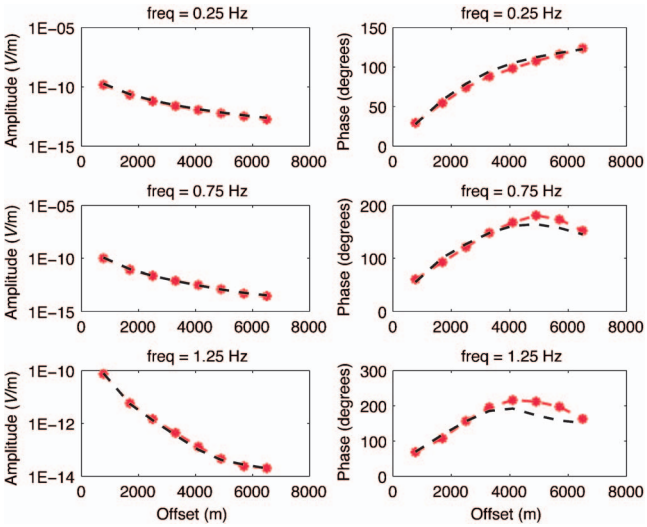

Figure 11. Observed CSEM data at receiver 16 and calculated data from EM inversion only. Red lines represent the field data, black lines represent the calculated data.

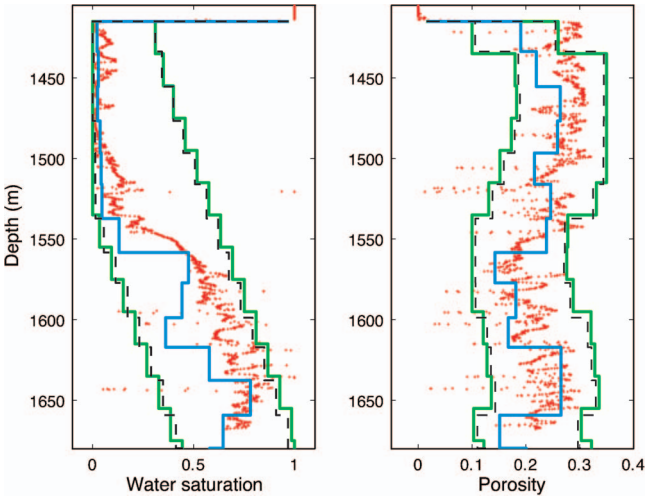

Figure 10. Inversion using EM data only. Red dots and lines represent well-log values, green lines are the prior bounds, blue lines are the estimated posterior modes, and black lines represent 99% predictive intervals.

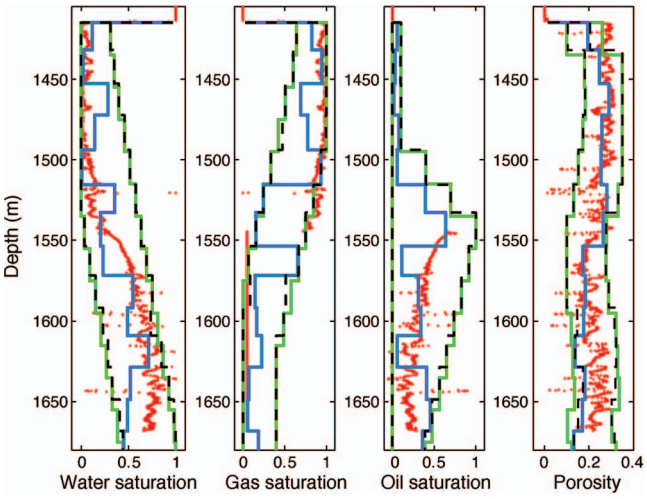

Figure 12. Joint inversion using seismic and EM data. Red dots and lines represent well-log values, green lines are the prior bounds, blue lines are the estimated posterior modes, and black lines represent 99% predictive intervals.

inversion using both types of data. The results are shown in Figures 13–15. By comparing these three figures with Figures 8, 10, and 12, respectively, we can see that the predictive intervals of almost all of the target parameters are much narrower because the ambiguity about these parameters has been reduced through the inclusion of the prior means. In addition to the narrower predictive intervals, the estimated posterior modes are closer to the well-log values. The improved posterior predictions are expected because more information is included when using the MRE approach to obtain the priors. It can be the case that information that is considered a suitable prior may in fact become incompatible with field observations as more observations become available. Our previous work (Hou and Rubin, 2005) studied the issues of prior incompatibility and showed that a heavy concentration of the posterior probability next to any of the prior bounds indicates such incompatibility.

By comparing the results from joint inversion (Figure 15) and seismic-only inversion (Figure 13), we can see that the inclusion of the CSEM data in the joint inversion improves the predictions of the target parameters with reduced predictive intervals and that the predictions of the gas saturations at the bottom layers of the reservoir are closer to the well-log observations.

The rms misfits between the inverted parameters and well-log observations, as well as the rms misfits between the CSEM/seismic AVA observations and the calculated model responses using inverted parameters are summarized in Table 1. For both uniform and truncated exponential prior PDFs, including CSEM data in the inversion reduces the rms misfits between the inverted parameters and the well logs. When using different combinations of seismic AVA and CSEM data, the more informative prior enables us to achieve smaller misfits. Another observation from the table is that the misfit between the seismic AVA observations and the calculated model responses becomes slightly larger, because the model fit for seismic AVA data is compromised by the inclusion of the CSEM data in the joint inversion.

In summary, the inclusion of EM data improves our estimates of water, gas, and oil saturations; it yields narrower predictive intervals as well as predictions that are generally closer to the well-log observations. The MRE-Bayesian framework enables us to deal with different types of prior information. Additional information, such as prior means, leads to much narrower predictive intervals of the target parameters as well as closer predictions to the well logs. Figure 16 shows the posterior distributions of the gas saturations at the third layer (gas-rich layer) and fifteenth layer (water-rich layer) from the top of the reservoir (e.g., 1405-m depth), illustrating the benefits of including the CSEM data and information about the prior means into the inversion procedure.

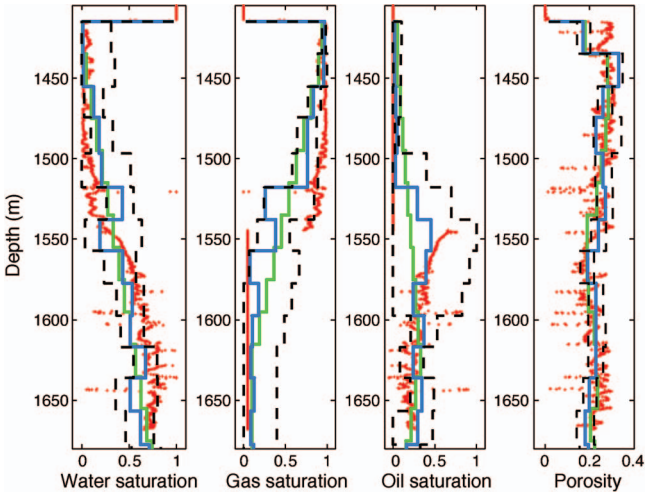

Figure 13. Inversion using only seismic data with information about prior means. Red dots and curve represent well-log values, green lines are the prior means, blue lines are the estimated posterior modes, and black lines represent 99% predictive intervals.

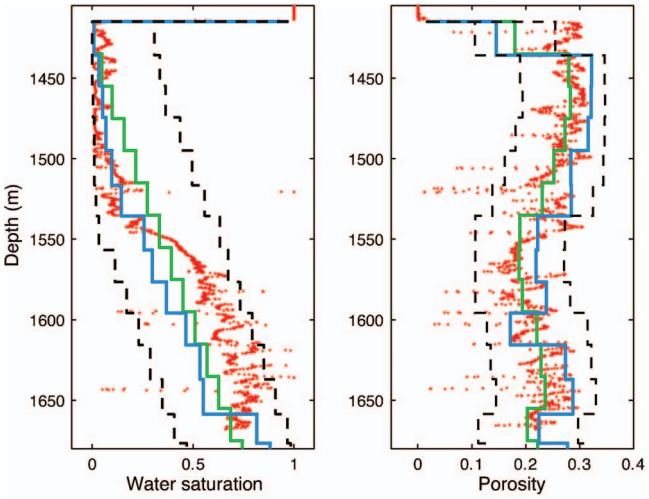

Figure 14. Inversion using only EM data with information about prior means. Red dots and curve represent well-log values, green lines are the prior means, blue lines are the estimated posterior modes, and black lines represent 99% predictive intervals.

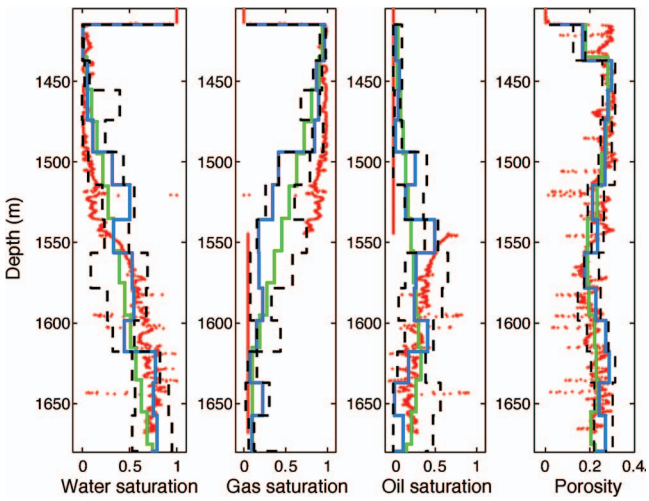

Figure 15. Joint inversion using seismic and EM data, with information about prior means. Red dots and curve represent well-log values, green lines are the prior means, blue lines are the estimated posterior modes, and black lines represent 99% predictive intervals.

Table 1. Root-mean-square misfits between the inverted parameters and well logs, rms misfits between the EM/seismic AVA observations, and the calculated model responses using inverted parameters.

		Rms misfit (S_w)	Rms misfit (S_g)	Rms misfit (S_o)	Rms misfit (porosity)	Rms of (S_w, S_g, S_o, and porosity)	Rms misfit (seismic AVA)	Rms misfit (CSEM)
Uniform prior	Seismic inversion	0.212	0.271	0.183	0.058	0.724	0.766	—
	EM inversion	0.198	0.238	0.210	0.064	0.710	—	0.217
	Joint inversion	0.170	0.257	0.155	0.058	0.640	0.888	0.155
Truncated exponential prior	Seismic inversion	0.163	0.219	0.145	0.057	0.584	0.686	—
	EM inversion	0.189	0.238	0.120	0.074	0.621	—	0.228
	Joint inversion	0.159	0.219	0.146	0.056	0.580	0.722	0.138

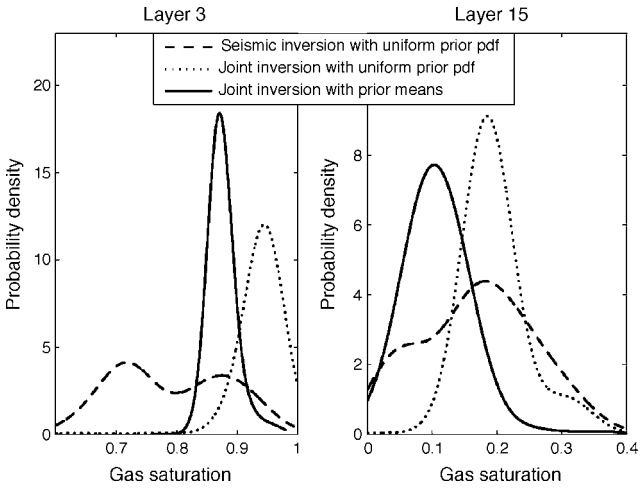

Figure 16. The posterior distributions of the gas saturations at the third layer (gas-rich layer) and fifteenth layer (water-rich layer) from the top of the reservoir (e.g., 1405 m depth).

CONCLUSIONS

We propose an MRE-Bayesian approach for joint seismic and EM inversion. Our preliminary results from synthetic data indicate that joint inversion based on seismic and EM data improves our capability to identify and confirm the locations of gas-rich layers. Seismic AVA responses can be used to identify the porosity very well. However, the responses are not sensitive to gas saturation changes; thus, incorporation of EM data in the inversion is warranted and is proven to be useful in improving our ability to predict gas saturation.

The approach is also applied to field data at Troll field in the North Sea. Results show the benefits of including EM data together with seismic data in the inversion. Compared to any individual inversion using either seismic or EM data, the joint inversion gives predictions that are generally closer to well logs and gives narrower predictive intervals, which means the ambiguity or uncertainty associated with the parameters is reduced.

The advantage of formulating this inverse problem in a stochastic framework is manifested in the statistics of the target parameters. Instead of the usual single-valued estimation that is provided by the deterministic approach, we obtain a probability distribution, which allows computing mean, mode, and confidence intervals and is useful for a rational evaluation of uncertainty and its consequences. Moreover, the MRE-Bayesian framework enables us to achieve much better parameter-estimation results when implementing a more informative prior.

We made several important assumptions in the study. We assumed the earth can be represented by a 1D layered model. This assumption may be inappropriate for high-frequency EM data sets at large offsets, because higher frequency EM responses are more easily affected by 3D structures of the earth. For seismic data, we assumed that the effects of multiples and waveform spreading can be neglected. We also assumed that the rock-physics model parameters developed from the well logs nearby are true for our study site. These assumptions can be overcome by increasing the complexity of both the seismic and EM models. For example, we can use 1D elastic-seismic calculation with waveform spreading, mode conversions, and all multiples; or we can consider quasi-2D, 2D, or even 3D forward models.

ACKNOWLEDGMENTS

The work is supported by the Research Partnership to Secure Energy for America (RPSEA) and the Assistant Secretary for Fossil Energy, National Petroleum Office of the U.S. Department of Energy, under contract DE-AC03-76SF00098. This work is also supported by NSF grant EAR-0450367 to Y. Rubin.

We are grateful to Statoil for supplying the CSEM data over Troll and to EMGS and Shell for their contributions of data and consultations. In particular, we thank Tage Rosten of Statoil, Jaap Mondt and Maren Kleemeyer of Shell, and Rune Mittet of EMGS. In addition, we thank the Troll partners (Norsk Hydro, Statoil, Petoro, Norske Shell, Total, and ConocoPhillips) for permission to publish this work.

APPENDIX A

QUASI-MONTE CARLO INTEGRATION OF NONLINEAR FUNCTIONS

As shown in equations 1 and 6, to get the posterior PDF and the posterior moments, integrations of nonlinear functions need to be carried out using Monte Carlo integration coupled with the concept of importance sampling. Here, a quasi-Monte Carlo method is used (Ueberhuber, 1997, p. 125). Quasi-Monte Carlo integration is a method of numerical integration that uses sequences of quasi-random numbers to compute the integral. Quasi-random numbers are generated algorithmically by computer and are similar to pseudorandom numbers, while having the additional important property of being deterministically chosen based on equidistributed sequences in order to minimize errors. It moves rapidly and smoothly to finer scales with increasing samples. One does not need to decide in advance how fine the grid should be; the method can sample until some convergence or termination criterion is met.

REFERENCES

Archie, G. E., 1942, The electrical resistivity log as an aid in determining some reservoir characteristics: Transactions of the American Institute of Mining, Metallurgical and Petroleum Engineering, **146**, 54–62.

Batzle, M., and Z. Wang, 1992, Seismic properties of pore fluids: Geophysics, **57**, 1396–1408.

Buland, A., and H. More, 2003, Bayesian linearized AVO inversion: Geophysics, **68**, 185–198.

Castagna, J. P., 1993, AVO Analysis—Tutorial and review, *in* J. P. Castagna and M. M. Backus, eds., Offset-dependent reflectivity—Theory and practice of AVO analysis: SEG Investigations in Geophysics 8, 3–36.

Chen, J., G. M. Hoversten, D. W. Vasco, Y. Rubin, and Z. Hou, 2004, Joint inversion of seismic AVO and EM data for gas saturation estimation using a sampling-based stochastic model: 74th Annual International Meeting, SEG, Expanded Abstracts, 236–239.

Debski, W., and A. Tarantola, 1995, Information on elastic parameters obtained from the amplitudes of reflected waves: Geophysics, **60**, 1426–1436.

Dvorkin, J., and A. Nur, 1996, Elasticity of high-porosity sandstones, Theory for two North Sea datasets: Geophysics, **61**, 1363–1370.

Eidsvik, J., H. Omre, T. Mukerji, G. Mavko, P. Avseth, and N. Hydro, 2002, Seismic reservoir prediction using Bayesian integration of rock physics and Markov random fields: A North Sea example: The Leading Edge, **21**, 290–294.

Ellingsrud, S., T. Eidesmo, S. Johansen, M. C. Sinha, L. M. MacGregor, and S. Constable, 2002, Remote sensing of hydrocarbon layers by seabed logging (SBL): Results from a cruise offshore Angola: The Leading Edge, **21**, 972–982.

Hashin, Z., and S. Shtrikman, 1963, A variational approach to the elastic behavior of multiphase materials: Journal of Mechanics and Physics of Solids, **11**, 127–140.

Hou, Z., and Y. Rubin, 2005, On minimum relative entropy concepts and prior compatibility issues in vadose zone inverse and forward modeling: Water Resources Research, **41**, W12425.

Hoversten, G. M., F. Cassassuce, E. Gasperikova, G. A. Newman, Y. Rubin, Z. Hou, and D. Vasco, 2006, Direct reservoir parameter estimation using joint inversion of marine seismic AVA and CSEM data: Geophysics, **71**, C1–C13.

Hoversten, G. M., R. Gritto, J. Washbourne, and T. M. Daley, 2003, Pressure and fluid saturation prediction in a multicomponent reservoir, using combined seismic and electromagnetic imaging: Geophysics, **68**, 1580–1591.

Hoversten, G. M., and M. Unsworth, 1994, Subsalt imaging via seaborne electromagnetics: Proceedings, Offshore Technology Conference, **26**, 231–240.

Johansen, S. E., H. E. F. Amundsen, T. Rosten, S. Ellingsrud, T. Eidesmo, and A. H. Bhuyian, 2005, Subsurface hydrocarbons detected by electromagnetic sounding: First Break, **23**, 31–36.

Landro, M., 2001, Discrimination between pressure and fluid saturation changes from time-lapse seismic data: Geophysics, **66**, 836–844.

Plessix, R., and J. Bork, 2000, Quantitative estimation of VTI paramenters from AVA responses: Geophysical Prospecting, **48**, 87-108.

Rubin, Y., 2003, Applied stochastic hydrogeology: Oxford Univ. Press, Inc.

Shuey, R. T., 1985, A simplification of the Zoeppritz equations: Geophysics, **50**, 609–614.

Spies, B. R., 1989, Depth of investigation in electromagnetic sounding methods: Geophysics., **54**, 872–888.

Tseng, H., and K. Lee, 2001, Joint inversion for mapping subsurface hydrological parameters: 71st Annual International Meeting: SEG, Expanded Abstracts, 1341–1344.

Ueberhuber, C. W., 1997, Numerical computation 2: Methods, software, and analysis: Springer-Verlag Berlin.

Ward, S. H., and G. W. Hohmann, 1987, Electromagnetic theory for geophysical applications *in* M. N. Nabighian, ed., Electromagnetic methods in applied geophysics, vol. 1. Theory: SEG Investigations in Geophysics 3, 131–228.

Woodbury, A. D., and T. J. Ulrych, 1993, Minimum relative entropy: Forward probabilistic modeling: Water Resources Research, **29**, 2847–2860.